Nuclear Materials and Energy 19 (2019) 295–299

Contents lists available at ScienceDirect

Nuclear Materials and Energy

journal homepage: www.elsevier.com/locate/nme

Plasma fluctuations in the scrape-off layer and at the divertor target in Alcator C-Mod and their relationship to divertor collisionality and density shoulder formation

A.Q. Kuang[a,*], B. LaBombard[a], D. Brunner[a,b], O.E. Garcia[c], R. Kube[c], A. Theodorsen[c]

[a] Plasma Science and Fusion Center, Massachusetts Institute of Technology, Cambridge, MA 02139, USA
[b] Commonwealth Fusion Systems, Cambridge, MA 02139, USA
[c] Department of Physics and Technology, UiT The Arctic University of Norway, N-9037 Tromsø, Norway

A B S T R A C T

Experiments indicate that the formation of density shoulders in the far scrape-off layer (SOL) is associated with an increase in cross-field transport and the propagation of coherent structures of high density known as blobs. It has been suggested that far SOL divertor collisionality (Λ_{div}) may be a controlling parameter in this physics, which could be challenging for heat flux mitigation schemes. At Alcator C-Mod, a new high spatial resolution divertor Langmuir probe array (rail probes) combined with a scanning Mirror Langmuir probe has been used to investigate this phenomenon in detail. Experiments were performed to mitigate divertor heat flux and thus increase Λ_{div} by two different methods and observe the divertor and scrape-off layer plasma response: (1) a 3-point density scan is found to increase the fluctuation intermittency at both the midplane and divertor, and produce a density shoulder at elevated Greenwald fraction; (2) a 3-point N_2 seeding scan is found to increase the divertor strike point collisionality, by over two orders of magnitude yet no noticeable trend is observed in either the density profile or the fluctuation statistics. It is concluded that Λ_{div} near the strike point is not by itself a controlling parameter for SOL fluctuations and shoulder formation which is important for localized heat flux mitigation schemes targeting the strike point where heat flux is the greatest.

1. Introduction

The density profile in the SOL on the low-field side (LFS) of a tokamak is characterized by a near SOL region with a relative short e-folding length and a far SOL region with a significantly longer e-folding length [1,2]. The separation point is often referred to as the break point. It has been observed at Alcator C-Mod that as the core plasma density is raised and approaches the global density limit (n_g), the far SOL e-folding length increases, often referred to as flattening, and the break point moves closer to the last closed flux surface (LCFS), also known as broadening [3]. These phenomena can lead to the increased erosion of and heat flux to the main chamber walls. Further analysis has shown that the flattening and broadening of the density profile is inconsistent with diffusive transport and is likely advective [1–8]. At higher core plasma densities, an increase in fluctuation amplitude was found to be correlated with the flattening and broadening of the profiles across multiple machines [9–12]. These large amplitude fluctuations have been observed to be due to coherent structures in the SOL that propagate both poloidally and radially across flux surfaces [13–15]. They have been found to be field aligned and to stretch from the midplane to the divertor [16–19]. These localized regions of high density are referred to in literature interchangeably as blobs or filaments due to their structure and appearance on diagnostics. The radial transport associated with these blobs has thus been termed blobby transport and is a function of the blob amplitude, velocity, and frequency of occurrence [20].

It is widely accepted that the blobs become polarized due to curvature and gradient driven particle drifts and are propelled radially outwards via the resulting E × B drift [15,16,21–23]. The amplitude of the polarization, and thus the blob velocity, is determined by the effective resistance to current flowing both parallel and perpendicular to the magnetic field lines within the filament. At low collisionality, the current closure pathway is through the plasma sheath at the divertor target. In this case, the filament is said to be 'electrically connected' to the divertor. In this regime, the cross field velocity is relatively low. At higher collisionality, the filament is 'electrically disconnected' from the divertor due to the increased resistivity in the divertor and the cross field velocity increases. An expression for the collisionality in a filament has been defined as [22]

$$\Lambda = \frac{L_{\parallel}\nu_{ei}}{\rho_s \Omega_{ce}} \tag{1}$$

where $L_{\parallel}$ [m] is the connection length from the LFS midplane to the divertor target, ν_{ei} [1/s] is the electron-ion collision frequency, ρ_s [m] is

* Corresponding author.
E-mail address: aqkuang@mit.edu (A.Q. Kuang).

https://doi.org/10.1016/j.nme.2019.02.038
Received 27 July 2018; Received in revised form 11 February 2019; Accepted 27 February 2019
Available online 15 March 2019

the ion sound speed Larmor radius, and Ω_{ce} [1/s] is the electron cyclotron frequency.

Recent theoretical analysis suggests that the arrival of blobs at a given point in the SOL can be represented as the sum of individual uncorrelated events. This model compares very favorably with experimental measurements [24–26]. An extension to this model, to include the cross field velocity of each filament, suggests that the flattening and broadening of the SOL density profile is likely due to either a reduction in parallel particle loss to the divertor within a filament as it propagates radially outwards or an increase in cross field velocity [27–30].

Carralero et al., [31] showed that, across a set of L-mode discharges spanning ASDEX and JET, the far SOL e-folding length organized well with Λ_{div}, which is Λ evaluated using divertor background plasma conditions. Note that, Carralero et al. further defined Λ_{div} to be evaluated in the far SOL and included an additional factor of 1/5 as a proxy for estimating the connection length from the X-point to the divertor [32]. The e-folding length and blob size increased significantly for $\Lambda_{div} > 1$ and was accompanied by a corresponding switch in the blob velocity scaling with size. Further experiments to determine the relationship between Λ_{div} and the density shoulder were performed at ASDEX [32], JET [33], and TCV [34] and in general they seemed to conclude that $\Lambda_{div} > 1$ was a necessary but insufficient condition for shoulder formation.

This result is important because heat flux mitigation schemes to protect the divertor inadvertently result in an increase in divertor collisionality due to the decrease in divertor plasma temperature. Given the already challenging task of mitigating divertor heat flux in future reactors, the difficulty would only increase if such efforts were coupled by filamentary transport to the main chamber. With the aim of investigating these and other SOL transport phenomena in Alcator C-Mod, a high poloidal resolution array of flush mounted and toroidally elongated rail Langmuir probes [35,36] were installed in the outer divertor. Together with the existing ~1 MHz high time resolution mirror Langmuir probe (MLP) system installed on a scanning probe at the outer midplane [37,38], experiments were performed on Alcator C-Mod to investigate fluctuation statistics at both midplane and divertor target locations and to examine their relationship to divertor collisionality and shoulder formation. This paper presents results from two sets of experiments in which divertor heat flux was reduced by: (1) increasing core plasma density which increased Λ_{div} across the entire SOL; and (2) performing N_2 seeding in the divertor which results in a localized increase in $\Lambda_{div}$for the near SOL. As the core plasma's density was raised, a density shoulder was observed and seen to flatten and broaden with increasing Greenwald fraction. Coincidently, the fluctuations became more intermittent. On the other hand, no change was seen in either the midplane density profile or fluctuation statistics when N_2 seeding was used to increase near SOL Λ_{div}. Section 2 outlines the diagnostics and techniques used to analyze the data; Section 3 compares results from 6 representative discharges; Section 4 discusses the resulting fluctuation statistics measured in the divertor and upstream; Section 5 summarizes the principle findings and discusses future work.

2. Alcator C-Mod boundary diagnostic suite

Fig. 1 shows the location of the rail Langmuir probe system and the MLP. The rail probe system consists of a poloidal array of 21 Langmuir probes that provide spatially well resolved profiles of divertor conditions. The probes were biased from −150 V to 50 V with a 200 Hz triangular voltage waveform. To obtain long time series ion saturation current density (J_{sat}) signals for fluctuation statistics analysis, each I-V characteristic was truncated for just the J_{sat} section, the minimum voltage at which $J = 0.95J_{sat}$ was first found (V_{cutoff}). Then the time segment corresponding to $V < V_{cutoff}$ for that I-V characteristic was extracted. A normalized current density signal was computed according to [39]

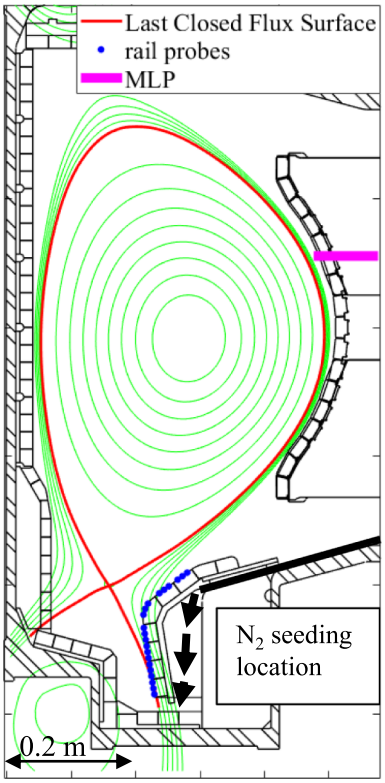

Fig. 1. Poloidal cross-section of the Alcator C-Mod tokamak with the location of diagnostics marked. The green contour lines are flux surfaces for a typical discharge and the red contour is the last closed flux surface. The divertor N_2 seeding location is indicated by the black lines and arrows. (For interpretation of the references to color in this figure legend, the reader is referred to the web version of this article.)

$$\tilde{J} = \frac{J - <J>}{J_{std}} \tag{2}$$

where $<J>$ is the signal mean and J_{std} is the signal standard deviation. Each normalized segment was then binned into 1 mm width bins that corresponded to their $\rho = R–R_{sep}$ coordinate when mapped to the outer midplane. Divertor fluctuations shown in this study were taken from $7 \leq \rho \leq 8$ mm except for discharge 6 (Table 1) which used $6.5 \leq \rho \leq 7.5$ mm as the original bin fell between probes.

To facilitate a comparison with divertor fluctuations, J_{sat} signals from the MLP scanning probe were processed in the following way. For each MLP scan, the far SOL segment corresponding to $7 \leq \rho \leq 11$ mm (up to the limiter position) was normalized as shown in Eq. (2) but with a moving window mean and standard deviation to compensate for drifts in the background plasma. A 1 ms moving window was applied which corresponded to ~100 times the typical fluctuation autocorrelation times (~10 μs) previously measured for the Alcator C-Mod SOL [3].

Table 1
List of discharges analyzed. Discharge 1–3 formed the density scan and discharge 4–6 formed the N_2 seeding scan. The divertor surface heat flux is included to indicate the level of heat flux mitigation achieved with the N_2 seeding.

Discharge	n/n_g	Seeding	Divertor q_{surf} ($q_{\|}$) [MW/m^2]
1	0.17	None (unmitigated)	4 (230)
2	0.23		3.7 (180)
3	0.29		3 (130)
4	0.27		3.5 (150)
5	0.27	N_2	2 (70)
6	0.27	N_2	0.5 (40)

3. Density and N_2 seeding scans used to mitigate divertor heat flux and thus vary Λ_{div}

The discharges compared in this study are listed in Table 1. All discharges were deuterium-fuelled, L-mode lower single null, with an on-axis magnetic field of 5.4 T and a plasma current of 0.8 MA. Discharges 1–3 form the 3-point density scan and discharges 4–6 form the 3-point N_2 seeding scan where core density and power into the SOL were held constant. The N_2 seeding level was maintained through a feedback control system developed for divertor heat flux control [40,41]. Shown in Table 1 are the divertor surface heat flux (q_{surf}) levels that were achieved with N_2 seeding, higher seeding levels resulted in lower q_{surf}. These were measured using the surface thermocouples [42] that were used as sensors for the feedback control. For ease of comparison to other devices, parallel heat fluxes ($q_{\parallel}$) are also shown in parenthesis. On Alcator C-Mod, $q_{\parallel} \approx 50\ q_{surf}$. Note that due to the closed divertor region of Alcator C-Mod, the effects of divertor nitrogen seeding is localized to the near SOL where plasma heat flux is the highest.

All discharges shown have attached divertor conditions. Although similar, the magnetic topology used for the density scan and the N_2 seeding scan were not identical. In particular, to mitigate heat fluxes on the outer divertor, a strike point sweep was employed for the density scan discharges but not for the N_2 seeding scan.

4. Comparison of SOL profiles and fluctuations statistics

Shown in Fig. 2 are the SOL profiles from the midplane and the divertor. The midplane density profiles in the density scan (top left plot) clearly flatten and broaden as the core density is increased but there is no discernible change to the density profiles in the N_2 seeding scan (top right plot). The e-folding length fitted to the far SOL ($4 < \rho < 8$ mm) was 9, 11, and 54 mm for increasing core density levels in the density scan and 8, 12 and 10 mm for increasing nitrogen seeding level in the N_2 seeding scan. Comparing divertor conditions we see that, as the core density is raised, density increases and the temperature decreases in the divertor resulting in an increase in collisionality (Λ_{div}) near the strike point of the divertor target. In the far SOL of the high density discharge (discharge 3), there is significant scatter in the T_e values due to increased fluctuation levels in the current recorded by the divertor Langmuir probes. In comparison, the effect of N_2 seeding is found to be more localized to the strike point, perhaps due to the closed divertor geometry in Alcator C-Mod. The seeding causes the density to rise and temperature to drop at the strike point, increasing the near SOL Λ_{div} by over a factor of 100. Note that similar to Carralero et al., Λ_{div} here is calculated using Eq. (1) but evaluated using divertor conditions with an additional factor of 1/5. However, as the intent is to show the variation in the entire profile across the SOL and highlight the different effects from the density scan versus the N_2 scan, Λ_{div} was calculated at all locations. There is a significant jump in the far SOL density e-folding length for the discharge 3 (the highest density discharge of the density scan) that corresponds with $\Lambda_{div} \approx 1$ at $\rho = 5$ mm. This is consistent with the behavior seen before and has been noted previously in [1,9,10,31,32].

Using the scheme outlined in Section 2, the skewness (S) and excess kurtosis (K) was calculated from the normalized signals of the 6 discharges [24]. The S and K values calculated from the signals are shown in Fig. 3, overall there appears to be an increasing trend in S and K values with density. This however appears to be weighted heavily by the higher density data points since looking at just the data points at $n_e/n_g \sim 0.17$ and 0.23 we find the slope to be only slightly increasing (divertor) or near constant (midplane). This trend is consistent with another study done by Kube et al. where the calculated S and K values at lower Greenwald fraction are similar before increasing at higher

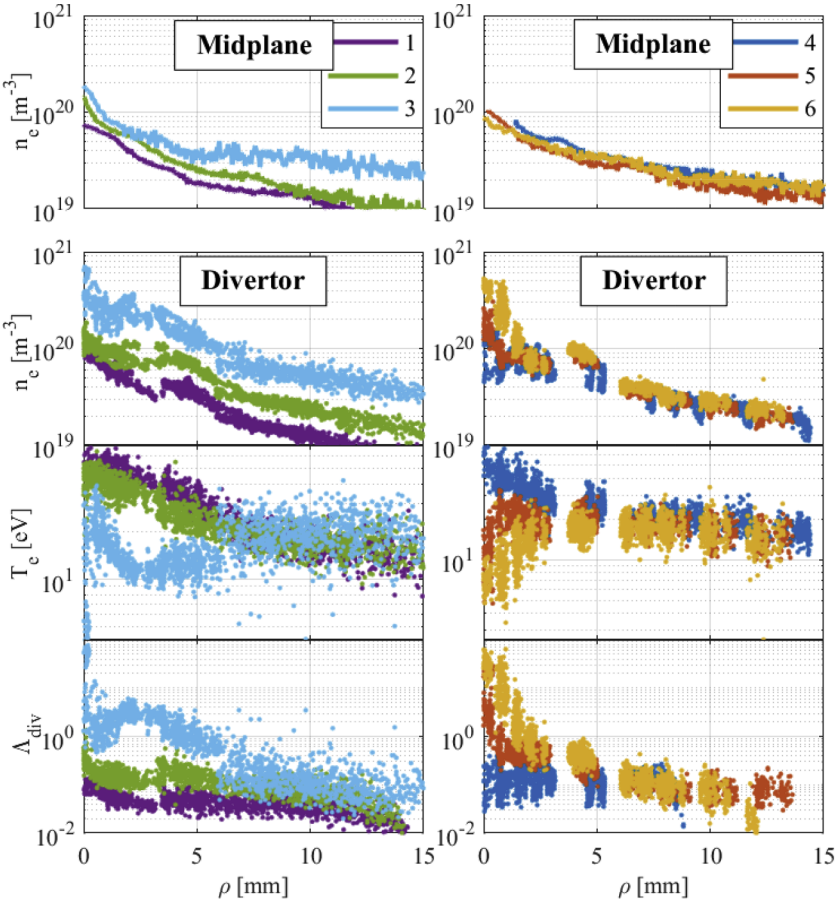

Fig. 2. The midplane density profile is shown in the top row of plots followed by the divertor density, temperature and Λ_{div}. The left column is the density scan and the right column is the nitrogen seeding scan. A clear flattening and broadening of the midplane density profile can be seen in the density scan but no discernible change can be observed in the N_2 seeding scan despite a near 100 fold increase in divertor strike point Λ_{div}. (For interpretation of the references to color in this figure legend, the reader is referred to the web version of this article.)

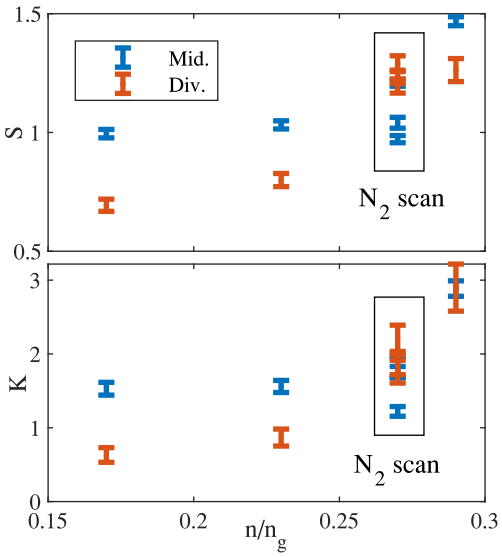

Fig. 3. Skewness (top) and excess kurtosis (bottom) increase with Greenwald fraction. (For interpretation of the references to color in this figure legend, the reader is referred to the web version of this article.)

Greenwald fractions [43]. Note that in that study, the density scan was performed at 0.5 MA while the discharges here were done at 0.8 MA. The similarities between the two studies support the findings by La-Bombard et al. that the main chamber SOL cross field transport correlates well with Greenwald fraction on Alcator C-Mod [9]. Based on Garcia's stochastic model, the fluctuations in the SOL follow a Gamma distribution which can be parameterized by an intermittency parameter (γ). A decreasing value of γ corresponds to larger and more distinct fluctuations captured statistically by an increasing S and K value [39]. To verify the observed trend in S and K, we use a second independent method to compute γ by fitting a Gamma distribution to a histogram of the fluctuation signals. γ calculated for the three density scan discharges at ($n_e/n_g \sim 0.17, 0.23, 0.29$) gives $\gamma_{mid} = 3.6, 2.7, 1.5$ and $\gamma_{div} = 3.7, 2.3, 1.5$ respectively, showing a clear decreasing trend consistent with the observed increase in S and K. In contrast, there is no clear trend with the N_2 seeding scan. Shown in Fig. 5 are histograms of the fluctuations from the N_2 seeding scan; overlaid is a gamma distribution function with intermittency parameter, $\gamma = 3$. Note that this corresponds to $S = 1.15$ and $K = 2$ [30]. There are some changes to the fluctuation statistics but it does not increase monotonically with increasing N_2 seeding levels.

Note that to ensure convergence of S and K and determine their uncertainty, a random subset containing 75% of the data from each time signal was selected and used to calculate S and K. This was repeated 20,000 times to obtain a distribution for S and K and the error bars indicate two standard deviations about the mean [44]. It is important to note that flush mounted probes are not traditionally used as a diagnostic for plasma fluctuations due to complication from sheath expansion effects. It is made possible in this analysis due to the unique design of the rail probes which has been shown to effectively mitigate sheath expansion [35,36]. Therefore, to check that the fluctuation statistics have been calculated correctly, the calculated S and K values were compared against the parabolic relationship often seen in experiment and theoretically derived in [24] (Fig. 5). The divertor fluctuations measured using the rail probes (red and black data points) show the same amount of scatter about the theoretical scaling (solid black line) as the midplane fluctuation measurements (green and blue data points), an indication that they are not being skewed by sheath expansion effects.

It is important to point out that fluctuation signals reported by the new flush-mounted rail probe are more consistent with midplane

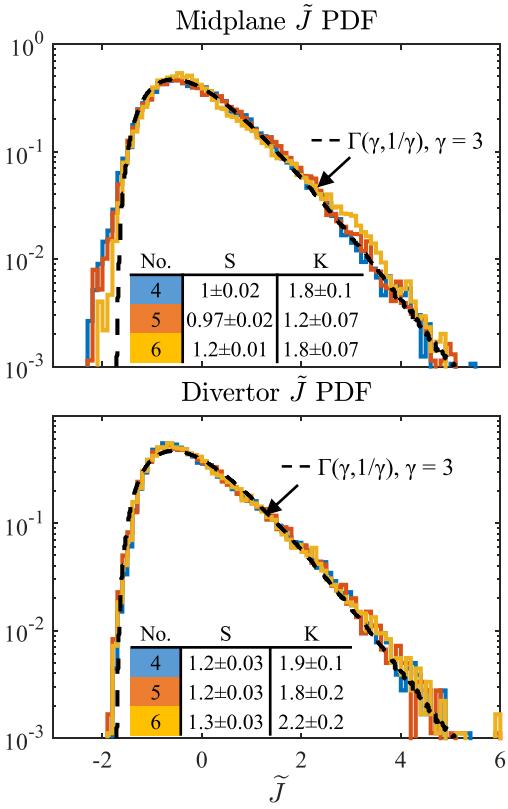

Fig. 4. Normalized histogram of the N_2 seeding scan fluctuation signals. There is no clear trend of S and K with increasing N_2 seeding levels. The fluctuations align well with the gamma distributed pdf overlaid.

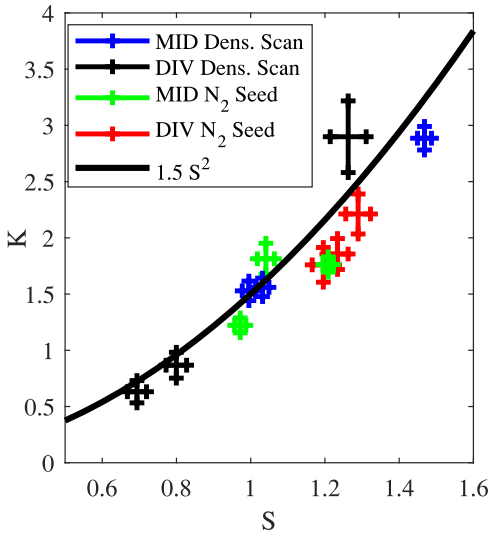

Fig. 5. The skewness and excess kurtosis calculation from the fluctuation signals organize well with the establish parabolic relationship. (For interpretation of the references to color in this figure legend, the reader is referred to the web version of this article.)

fluctuation measurements than with the old proud probe array used previously [39]. In this analysis of the proud probes, it was noted that the divertor fluctuation statistics lacked elevated tails. In comparison, as seen in Fig. 4, histograms of midplane and divertor fluctuations measured with rail probes are nearly identical. Apparently, proud probes are not able to capture fast, large amplitude bursts [45]. The root cause for this discrepancy remains unknown at this time.

Based on the increase in S and κ we conclude that the fluctuations

become more intermittent as the density is raised. In contrast, there is no change to the blobs in the N_2 seeding scan. The lack of a change in the fluctuation statistics in the far SOL for the N_2 seeding scan is a strong indicator that the blob dynamics are not being changed by the changes to the strike point divertor conditions. Note that there is little to no change to the local divertor conditions in the far SOL during the N_2 seeding scan. In comparison, as core density is increased there is a clear increase in far SOL Λ_{div}. However, it is not possible to determine if the Λ_{div} in the far SOL is playing any significant role; it may be simply increasing in response to the density shoulder formation. Ideally, future experiments could increase the far SOL Λ_{div} while keeping core parameters constant. Since no further experiments are planned for Alcator C-Mod, such investigations would need to use other facilities.

5. Conclusion and future work

Using the recently installed divertor rail probes and the midplane MLP, we recover the flattening and broadening of the midplane density profile as core plasma density is increased as previously reported. In addition, fluctuations measured at both the midplane and divertor target far SOL become more intermittent. These observations are correlated with an increase in Λ_{div} in the far SOL as previously reported. We find however that when the near SOL Λ_{div} is increased using divertor N_2 seeding, there is no change to the midplane density profile or to the fluctuations at the midplane and in the divertor. This is important for the development of heat flux mitigation schemes, as it indicates that changing divertor strike point and near SOL plasma conditions, where $q_{\parallel}$ is the greatest, would not affect midplane profiles. All calculated values of skewness and excess kurtosis agree with established relationships and the histograms of the measured fluctuations follow a gamma distribution.

Future work includes comparing fluctuation statistics in detached and attached conditions, as well discharges with different plasma currents. Furthermore, making use of the MLP system, fluctuation induced particle fluxes will be explored.

Acknowledgements

This work was supported by USDoE Coop. Agreement DE-FC02-99ER54512 on Alcator C-Mod, a DoE Office of Science user facility. This work was supported with financial subvention from the Research Council of Norway under grant 240510/F20.

References

[1] B. LaBombard, M. Umansky, R. Boivin, J. Goetz, J. Hughes, B. Lipschultz, D. Mossessian, C. Pitcher, J. Terry, Nucl. Fusion 40 (2000) 2041.
[2] B. Lipschultz, D. Whyte, B. LaBombard, Plasma Phys. Control. Fusion 47 (2005) 1559.
[3] B. LaBombard, et al., Phys. Plasmas 8 (2001) 2107.
[4] D. Whyte, B. Lipschultz, P. Stangeby, J. Boedo, D. Rudakov, J. Watkins, W. West, Plasma Phys. Control. Fusion 47 (2005) 1579.
[5] J.A. Boedo, et al., Phys. Plasmas 8 (2001) 4826.
[6] G. Antar, S. Krasheninnikov, P. Devynck, R. Doerner, E. Hollmann, J. Boedo, S. Luckhardt, R. Conn, Phys. Rev. Lett. 87 (2001) 065001.
[7] M. Umansky, S. Krasheninnikov, B. LaBombard, J. Terry, Phys. Plasmas 5 (1998) 3373.
[8] O.E. Garcia, R. Pitts, J. Horacek, A. Nielsen, W. Fundamenski, J. Graves, V. Naulin, J.J. Rasmussen, J. Nucl. Mater. 363 (2007) 575.
[9] B. LaBombard, J. Hughes, D. Mossessian, M. Greenwald, B. Lipschultz, J. Terry, A.C.-M. Team, Nucl. Fusion 45 (2005) 1658.
[10] O.E. Garcia, R. Pitts, J. Horacek, J. Madsen, V. Naulin, A.H. Nielsen, J.J. Rasmussen, Plasma Phys. Control. Fusion 49 (2007) B47.
[11] F. Militello, P. Tamain, W. Fundamenski, A. Kirk, V. Naulin, A.H. Nielsen, Plasma Phys. Control. Fusion 55 (2013) 025005.
[12] D. Rudakov, et al., Nucl. Fusion 45 (2005) 1589.
[13] J. Terry, et al., Nucl. Fusion 45 (2005) 1321.
[14] S. Zweben, et al., Phys. Plasmas 13 (2006) 056114.
[15] S.I. Krasheninnikov, Phys. Lett. A 283 (2001) 368.
[16] D. D'Ippolito, J. Myra, S. Zweben, Phys. Plasmas 18 (2011) 060501.
[17] A. Kirk, B. Koch, R. Scannell, H. Wilson, G. Counsell, J. Dowling, A. Herrmann, R. Martin, M. Walsh, Phys. Rev. Lett. 96 (2006) 185001.
[18] O. Grulke, J. Terry, I. Cziegler, B. LaBombard, O. Garcia, Nucl. Fusion 54 (2014) 043012.
[19] R. Maqueda, D. Stotler, N. Team, Nucl. Fusion 50 (2010) 075002.
[20] D. Carralero, et al., Nucl. Fusion 58 (2018) 096015.
[21] J. Myra, D. D'ippolito, S. Krasheninnikov, G. Yu, Phys. Plasmas 11 (2004) 4267.
[22] J. Myra, D. Russell, D. D'Ippolito, Phys. Plasmas 13 (2006) 112502.
[23] D. Russell, J. Myra, D. D'Ippolito, Phys. Plasmas 14 (2007) 102307.
[24] O. Garcia, Phys. Rev. Lett. 108 (2012) 265001.
[25] O.E. Garcia, S.M. Fritzner, R. Kube, I. Cziegler, B. LaBombard, J.L. Terry, Phys. Plasmas 20 (2013) 055901.
[26] O.E. Garcia, A. Theodorsen, Phys. Plasmas 24 (2017) 032309.
[27] F. Militello, J. Omotani, Nucl. Fusion 56 (2016) 104004.
[28] N. Walkden, A. Wynn, F. Militello, B. Lipschultz, G. Matthews, C. Guillemaut, J. Harrison, D. Moulton, Plasma Phys. Control. Fusion 59 (2017) 085009.
[29] N. Walkden, A. Wynn, F. Militello, B. Lipschultz, G. Matthews, C. Guillemaut, J. Harrison, D. Moulton, J. Contributors, Nucl. Fusion 57 (2017) 036016.
[30] O.E. Garcia, R. Kube, A. Theodorsen, H. Pécseli, Phys. Plasmas 23 (2016) 052308.
[31] D. Carralero, et al., Phys. Rev. Lett. 115 (2015) 215002.
[32] D. Carralero, et al., Nucl. Fusion 57 (2017) 056044.
[33] A. Wynn, et al., Nucl. Fusion 58 (2018) 056001.
[34] N. Vianello, et al., Nucl. Fusion 57 (2017) 116014.
[35] A. Kuang, D. Brunner, B. LaBombard, R. Leccacorvi, R. Vieira, Nucl. Mater. Energy 12 (2017) 1231.
[36] A. Kuang, D. Brunner, B. LaBombard, R. Leccacorvi, R. Vieira, Rev. Sci. Instrum. 89 (2018) 043512.
[37] B. LaBombard, L. Lyons, Rev. Sci. Instrum. 78 (2007) 073501.
[38] B. LaBombard, T. Golfinopoulos, J. Terry, D. Brunner, E. Davis, M. Greenwald, J. Hughes, A.C.-M. Team, Phys. Plasmas 21 (2014) 056108.
[39] R. Kube, A. Theodorsen, O.E. Garcia, B. LaBombard, J.L. Terry, Plasma Phys. Control. Fusion 58 (2016) 054001.
[40] D. Brunner, W. Burke, A. Kuang, B. LaBombard, B. Lipschultz, S. Wolfe, Rev. Sci. Instrum. 87 (2016) 023504.
[41] D. Brunner, et al., Nucl. Fusion 57 (2017) 086030.
[42] D. Brunner, B. LaBombard, Rev. Sci. Instrum. 83 (2012) 033501.
[43] R. Kube, O. Garcia, A. Theodorsen, A. Kuang, B. LaBombard, J. Terry, D. Brunner, Nucl. Mater. Energy 18 (2019) 193.
[44] B. Efron and R.J. Tibshirani, An Introduction to the Bootstrap (CRC press, 1994).
[45] O.E. Garcia, A.Q. Kuang, D. Brunner, B. LaBombard, R. Kube, 59th Annual Meeting of the APS Division of Plasma Physics Milwaukee, WI, 2017, p. 194.